Physics and Technology in the Ion-cyclotron Range of Frequency on Tore Supra and TITAN test facility: implication for ITER

X. Litaudon, J.M. Bernard, L. Colas, R. Dumont, A. Argouarch, H. Bottollier-Curtet, S. Brémond, S.Champeaux[1],Y. Corre, P. Dumortier[2], M. Firdaouss, D. Guilhem, J.P. Gunn, Ph.Gouard[1], G.T. Hoang, J. Jacquot, C. C. Klepper[3], M. Kubič, G. Lombard, D. Milanesio[4], A. Messiaen[2], P. Mollard, O. Meyer, D. Zarzoso

CEA, IRFM, F-13108 St-Paul-Lez-Durance, France
[1] CEA, DAM, DIF, F-91297Arpajon, France
[2] Association EURATOM-Belgian State, TEC, Royal Military Academy, Brussels, Belgium
[3] Oak Ridge National Laboratory, Oak Ridge, TN 37831-6169, USA
[4] Department of Electronics, Politecnico di Torino, Turin, Italy

e-mail of first author: xavier.litaudon@cea.fr

Abstract. To support the design of ITER ion-cyclotron range of frequency heating system and to mitigate risks of operation in ITER, CEA has initiated an ambitious Research & Development program accompanied by experiments on Tore Supra or test bed facility together with a significant modeling effort. The paper summarizes the recent results in the following area:

- Comprehensive characterization of a new Faraday screen concept tested on Tore Supra antenna. RF sheath rectification is now better understood: a new model has been developed and applied to ITER.
- Full wave modeling of ITER ICRH heating and current drive scenarios with EVE code. With 20MW of power, a current of ±400kA could be driven on axis in the DT scenario.
- First operation of CW test bed facility, TITAN, designed for ITER ICRH components testing and could host up to a quarter of an ITER antenna.
- R&D of high permittivity materials to improve load of test facilities to mimic ITER plasma conditions.

1. Introduction

The ITER ion-cyclotron range of frequency (ICRF) heating system is required to couple 20MW of power in the frequency range 40-55MHz. The system should provide robust coupling for a variety of plasma scenarios with Edge Localised Modes. The coupling depends on plasma density in the scrape-off layer (SOL) which is not well known. Coupling and wave propagation predictions of the ion cyclotron waves require a prior knowledge of plasma properties and accurate modeling of the plasma wave propagation into the plasma edge and core. In poor coupling conditions, high voltage in the antenna will be required to radiate the full power. In the adverse conditions, the power will be limited by the maximum voltage that the antenna could sustain. To mitigate this risk on ITER, it is foreseen to install two port-plug antennas to radiate the same 20MW power but with two antennas on long pulse operation. In this context, operation of actively cooled ICRF systems on existing plasma devices together with a significant modeling effort and R&D programme on dedicated test bed facilities are of prime importance. CEA activity is reviewed in the field of modeling, experiments and technology, including (i) model validation on Tore Supra and extrapolation toward ITER, (ii) R&D on the new TITAN test bed facility (TITAN for Test-bed for ITER icrf ANtenna) for testing ITER ICRF components.
After this introduction, the paper is organized in four main sections. In section 2, we review the effort to better understand the RF-sheath rectification process that appears at the vicinity of the ICRH antenna. The challenge is to experimentally characterise and model the behaviour of a new Faraday screen installed on one of the Tore Supra antenna. A new model for the description of the non-linear RF-sheath rectification has been proposed and applied to both Tore Supra and ITER. In section 3, the full wave modeling of ITER ICRF heating and

current drive scenarios is presented focusing on the comparison of two scenarios in the activated phase of ITER. A new test stand facility, TITAN, has been installed at CEA/IRFM and its first operation is reported in section 4. Recent progress made on the design and development of a new plasma-like load with high permittivity materials using ferroelectric barium titanate $BaTiO_3$ ceramics is also reported in section 5.

2. RF-Sheath rectification: experiments and modeling for Tore Supra and ITER

The non-linear interaction of intense radio-frequency (RF) near fields in the ion cyclotron range of frequencies with the peripheral plasma is of major concern for ITER plasma facing components. Its most likely origin, RF sheath rectification, causes enhanced sputtering, increased heat fluxes and re-distribution of the Scrape-Off Layer, SOL, density. In aiming to reduce this interaction the challenge is to understand how the spatial topology of RF currents developing in the front face of the ICRF antennae influences the RF sheath patterns.
The simplest RF-sheath rectification models (e.g. [1]) treat independently each open flux tube in the SOL as a double Langmuir probe driven by an oscillating voltage, taken as the line-integrated parallel RF electric field $E_{//}$ evaluated in the absence of sheaths. Applying this model to minimize, $|\int E_{//}.dl|$ along "long field lines" with a large toroidal extension on both sides of the wave launcher, led to interrupting all parallel RF current paths on the antenna front face [2]. The resulting new Faraday Screen, FS, is shown on Fig. 1 (left) mounted on a two-strap Tore Supra antenna. Electrically it is characterized by a slotted frame with "shark teeth" and cantilevered horizontal rods, as opposed to tilted bars attached on their two sides on classical FS. The FS bars are also thicker and their number was reduced from 34 to 19 to conserve transparency. The central septum was retracted radially. The new FS is actively cooled on its bars, septum and lateral collectors. Its cooling scheme was revised to accommodate the new front face design and improve the heat exhaust [3].
Using IR thermography and 2D reciprocating Langmuir probe mapping, the RF-sheath spatial topology was extensively characterized on Tore Supra plasmas in relation with the strap and FS electrical properties. SOL plasma measurements revealed that the new FS neither reduced the measured probe floating potentials, V_f, (V_f up to 150V [4]) nor the RF-induced heat loads (350kW/m^2 on lateral collectors, 700kW/m^2 on FS rods [3], 5.0MW/m^2 parallel to $\mathbf{B_0}$ maximum on side limiters [5]). The power lost on FS side limiters, as estimated by calorimetry of the cooling water loops, is ~5% of the launched RF power with the new FS in $[0,\pi]$ phasing, versus 3.5% for classical one [6]. Despite these high fluxes, efficient cooling allowed operating the new antenna up to 3MW×6s. The heat loads with classical and new antenna share a two-hump poloidal variation with local maxima near the FS corners and minima on the equatorial plane along the side limiters, visible on Fig. 1 (right). Similar poloidal variation is observed on the probe floating potentials on Fig. 2 (left) [4]. Postulating that V_f is indicative of the DC plasma potential, $\mathbf{E}\times\mathbf{B_0}$ density convection is expected along the iso-potentials sketched on Fig. 2 (left). The main effects were observed on "short field lines" with screen-screen magnetic connections, or lateral flux tubes emerging from the antenna side limiters that were not envisaged in the $|\int E_{//}.dl|$ minimization.

Within an international collaborative framework, a new approach has been proposed to model self-consistently the interplay between the slow magnetosonic wave (SW) penetration and edge plasma DC biasing using a three-field fluid formulation: the SSWICH code [7-8]. The present geometry is restricted to a 3D collection of straight open field lines ended by walls normal to $\mathbf{B_0}$. A wave equation propagates radially a 2D (toroidal/poloidal) map of $E_{//}$ imposed at the low field side of the simulation domain. RF voltages are then excited by the RF electric field invoking the Sheath-Plasma Wave. The local DC plasma potential is

governed by the continuity equation for DC currents in presence of parallel and effective transverse DC conductivity. Sheaths at both ends of open flux tubes are described by RF and DC boundary conditions (SBCs). The non-linear I-V characteristic of the sheaths couples the RF and DC quantities. Rectification of $E_{//}$ acts as inhomogeneous positive DC biasing of the walls [8]. For RF waves, sheaths behave as thin dielectric layers between the plasma and the conducting walls, whose width depends on the DC plasma potential *via* Child-Langmuir law [9]. The physical model is implemented using the COMSOL Finite Element solver and a Newton-Raphson iterative algorithm. To ease convergence of the iterations, a first guess of the final solution is needed and is provided by an asymptotic version of SSWICH [8]. The asymptotic model assumes very large sheath widths, so that the RF-SBCs get simplified. The SW module can thus be solved explicitly without prior knowledge of the DC plasma potentials. The asymptotic model predicts that RF sheath voltages can propagate radially well beyond the skin depth characteristic of SW evanescence, and that they scale as $P_{RF}^{1/2}$.
The new SSWICH procedure has been applied for the first time to compare the two Tore Supra FS designs [7], using input RF excitation provided by the antenna code TOPICA without sheaths [10]. First simulations suggest that the new FS enhances RF sheaths instead of reducing them, in line with the experiments. The overall two-hump poloidal structure of the heat loads on side limiters could also be reproduced (see Fig. 2 (right)). While this poloidal distribution is a relatively robust output, the quantitative amplitudes and radial penetration of rectified DC potentials are found sensitive to loosely constrained simulation parameters: toroidal and radial extension of the private SOL; transverse plasma DC conductivity. However the simulated heat fluxes in the private SOL between the two side limiters are in the correct range: ~4MW/m^2 parallel to the field lines for 30kV strap voltage. Numerical investigation has neither identified yet which element of the new FS design enhances the sheaths. Possible candidates are: horizontal FS bar, electrical disconnection from the septum, greater gaps between rods. To sort out, it is proposed to modify these elements individually in the future simulations.

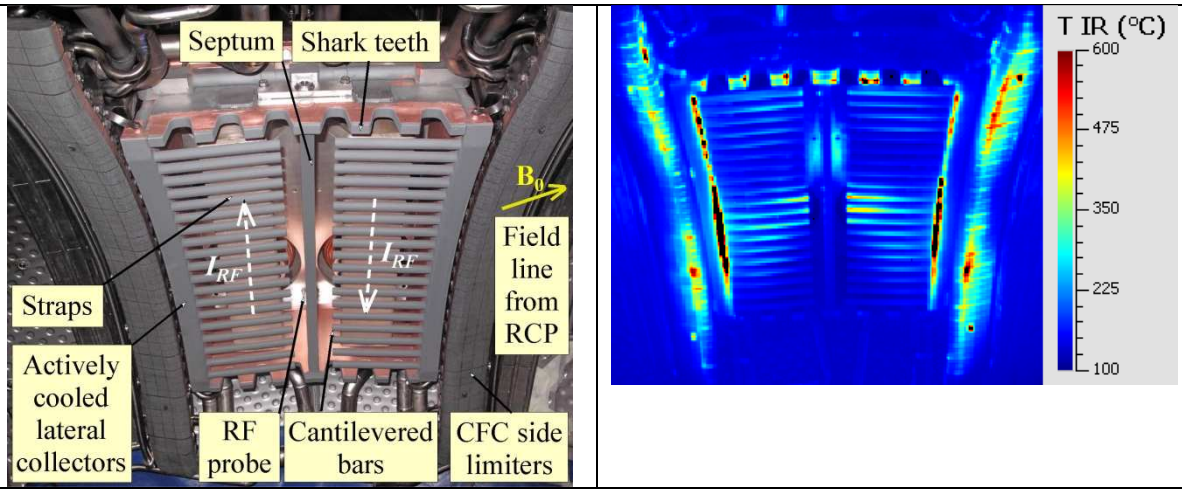

***Fig. 1**: (left) Picture of the new Faraday Screen mounted on a two-strap Tore Supra antenna. (right) Infrared image of new Faraday Screen at the end of the 3MW×6s RF pulse.*

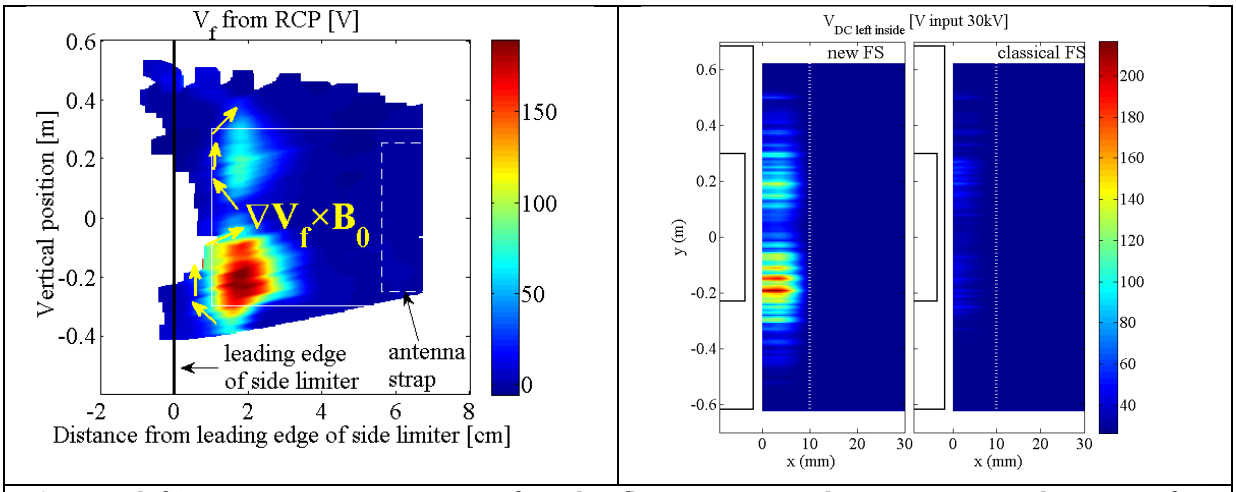

Fig. 2: *(left) Experiments: Mapping of probe floating potential V_f, versus 2D location of its connection point to the right side limiter of new Tore Supra antenna. Streamline of $\boldsymbol{E}\times\boldsymbol{B_0}$ convection in the gradient of V_f is superimposed. (right) 2D SSWICH simulation : (radial/poloidal) distribution of DC plasma potentials at inner side of left Tore Supra antenna limiters, (30kV RF voltage on straps). Left map with new FS, right with classical Tore Supra antenna. Also sketched is the vertical extension of antenna box and side limiters.*

The SSWICH model in its asymptotic form has been finally applied in a predictive way to estimate sheath effects on the Blanket Shielding Modules (BSM) surrounding the ITER ICRF antenna [11]. In order to provide an upper bound of sheath heat loads, a low-density SOL profile was used that was shifted radially by 8cm towards the wall, and the input RF field maps were normalized to 20MW RF power coupled. Most pessimistic estimated heat fluxes are in the range 6MW/m^2 parallel to $\mathbf{B_0}$. Estimated RF power losses over BSM edges are about 125kW. For overall losses a hierarchy of strap phasings emerges from the simulations: [0,0,π,π]>[counter-current drive phasing], [co-current drive phasing]>[0,π,π,0]>[0,π,0,π], which is reminiscent of experimental observations with the four-strap A2 antennae on JET [12]. This spatial distribution of parallel heat flux densities and its variation with strap phasing weakly depend on small changes of the antenna front face design ("CY8vr1S" vs "CY8vr2S") or on the type of strap excitation ("Istrap" vs "Vmax" excitation).

3. Full wave modeling of ITER ICRH heating & Current drive Scenarios

In parallel to the description of the antenna-SOL interaction, several aspects pertaining to the use of ICRF waves in the activated phase of ITER have been addressed using state-of-the art numerical tools [13]. In particular, ICRF waves have the capability of driving plasma current by direct damping of the fast magnetosonic wave by electrons. Owing to the absence of stringent accessibility limitation for the fast wave (FW), and to the availability of reliable RF generators in the ICRF, this method is attractive for next-step fusion reactors, including during H-mode operation [14]. On the other hand, FW current drive (FWCD) is known to be experimentally challenging due to the low absorptivity of the FW electron damping mechanisms and/or to parasitic damping of the wave by ions, even at rather high harmonics of the cyclotron resonance [15]. In ITER, the situation differs with respect to most past experiments [16], as no “pure” FWCD scheme is readily available. The simultaneous presence of multiple species and the magnetic configuration make it impossible to exclude all low harmonics cyclotron layers from the plasma in the foreseen frequency range for the ICRF system. Therefore, the idea is to take advantage of the high electron temperature in ITER plasmas, and exploit the ICRF waves whose primary goal is to heat the plasma in order to drive centrally peaked current. In this respect, the FW driven current may be considered as an

added value of the ICRF system. In the typical scenarios envisioned for ITER, the driven current profile is peaked on axis, and only its magnitude can be controlled within the limits defined by the maximum available power, the flexibility of the RF system in terms of toroidal phasing and the FWCD efficiency.

Two ICRF scenarios have been extensively compared i.e. i) second harmonic tritium heating (DT), and ii) helium 3 minority heating DT(^{3}He). Their practical implementations differ in that a small fraction of ^{3}He ions have been added in plasma in the latter case. This, however, is known to profoundly affect the ICRF scenario by improving the wave damping and also possibly the nuclear reaction rate, as was demonstrated in JET [17]. In each case, the performance of FWCD is analyzed in terms of current drive efficiency. The minimal set of ingredients required to address these points includes:

- A multi-dimensional full wave code able to compute the electromagnetic field excited by the antenna in the whole plasma volume. The Hamiltonian wave code EVE [18] is employed. Given the axisymmetric nature of the problem at hand, every toroidal mode is handled independently.
- A post-processor to recombine the solutions corresponding to individual toroidal numbers, appropriately weighted, and deduce the power split between species and the FW driven current (estimated using the heuristic Ehst-Karney formula [19, 20])
- A Fokker-Planck (FP) solver to evaluate the fast ion population features. For this purpose, EVE has been supplemented with a simplified FP module, named AQL [13].

The plasma parameters are based on those employed in a recent benchmark of full-wave codes presented in Ref. 21. The magnetic and kinetic equilibrium background plasma profiles are provided by the PTRANSP code. Eight ion species are taken into account: thermal deuterium, tritium, argon, beryllium, alphas, thermal ^{4}He, ^{3}He and deuterium beam. The plasma equilibrium is provided by the EFIT code. The ICRF antenna is located on the low field side, at midplane position R_{ant}=8.38m and the working frequency is f=52.5MHz. Superthermal species, namely alphas, D beam and the heated ion are modeled using equivalent anisotropic Maxwellians. In the simulation two power levels have been used, namely P_{RF}=20MW and P_{RF}=10MW. As an illustration, Fig. 3 (left) shows a comparison of the contours of the right-handed electric field magnitude in the DT case and in the DT(^{3}He) case, assuming a total absorbed power of 20MW and a [0,π/2,π,3π/2] phasing. It is clear that the addition of 2% of ^{3}He in the DT mixture results in improved per-pass damping. Whereas the power is roughly evenly split between tritium ions and electrons in the first scenario, a large fraction of the RF power (54.9%) is absorbed by the minority ions in DT(^{3}He), the remainder being absorbed by electrons (30.0%) and tritium ions (14.1%). In both cases, the alpha damping is weak (~1%). Superthermal ion tails may significantly affect the driven current profile through modification of the power split between species. In each simulation, the fast ion population is obtained using AQL, and a new solution for the ICRF wave field is computed by EVE. This iterative process between EVE and AQL is continued until a stationary solution is found, which usually occurs in less than 5 iterations. In Fig. 3 (right) is shown the profile of driven current when the [0,π/2,π,3π/2] phasing is used. In order to compare the results obtained for P_{RF}=10MW and P_{RF}=20MW, the driven current is normalized to P_{RF}. DT and DT(^{3}He) scenarios differ in the influence of quasilinear effects: whereas the tritium tail results in stronger ion absorption and thus lowers the amount of driven current level with increasing power in the former scenario, the FWCD efficiency is only moderately modified by quasilinear effects in the latter, as a result of the characteristics of minority damping.

In order to quantify the flexibility of the ITER ICRF system in terms of FWCD, a systematic study of various inter-strap phasings has been performed. We have considered the individual solutions computed by EVE for [0,π/2,π,3π/2] phasing and recombined them for various dipole-like phasings, i.e. phasings of the type [0,Δϕ/2,Δϕ,3Δϕ/2] with Δϕ varied between -π and π. We observe that the [0, ±π/2, ±π, ±3π/2] phasing is not the most efficient in terms of driven current. Phasings characterized by lower values of $\langle k_{//} \rangle$ where <> denotes averaging over toroidal numbers allow to drive more current, even though electron damping decreases. Overall, we find that it is possible to expect up to ~200kA with 10MW, and up to ~400kA with 20MW in the DT case. However, a trade-off needs to be found between plasma heating (and ion tail generation) and current drive, since the power split is modified by the phasing in a rather significant way. In this respect, the DT(^{3}He) scenario is more robust since ^{3}He damping always dominates. However, we note that the magnitude of the driven current is approximately half the magnitude obtained in the DT scenario. Defining the normalized efficiency $\eta_{FW}=J_{FW}/P_{RF}R_0n_{e,20}$ versus toroidal phasing (R_0 is the major radius, $n_{e,20}$ is the line-averaged electron density in units of $10^{20}m^{-3}$), FWCD efficiencies of the order ~0.015-0.025A/W are obtained in the DT scenario, corresponding to η_{FW}~0.1-0.2A/W/m^3. In the DT(^{3}He) case, the sensitivity to the total absorbed power is weak, but the efficiency is also lower: ~0.01A/W, corresponding to η_{FW}~0.05A/W/m^3.

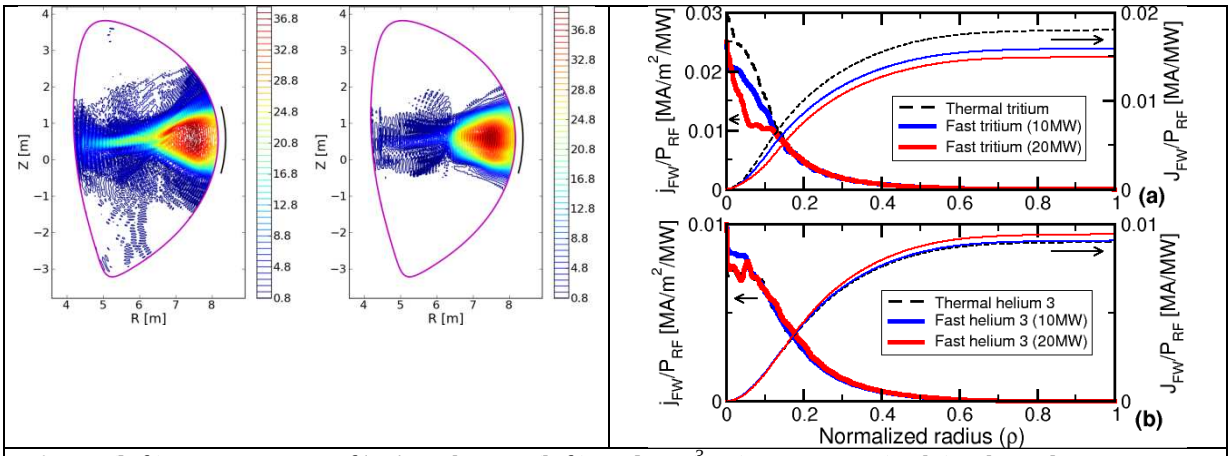

Fig. 3: (left) *Iso-contours of |**E**.| in the DT (left) and DT(^{3}He) scenarios (right). The values are given in kV/m for 20MW absorbed power and the antenna is in [0,π/2,π,3π/2] phasing. (right) Driven current profile (left y-axis) and cumulative current (right y-axis) per absorbed MW for [0,π/2,π,3π/2] phasing when the fast ion effects are neglected (dashed) or incorporated for a total absorbed power of 10MW or 20MW (solid) in the DT scenario (a), in the DT(^{3}He) scenario (b).*

4. New high power CW test facility for ITER ICRH components testing

Finally, in the framework of the ITER ICRF R&D program, the qualification of RF components requires dedicated facilities to provide relevant test conditions in terms of thermal cycling, vacuum and power. A new test stand facility, TITAN, has been installed at CEA/IRFM (Fig. 4 (left)) [22]. This is the first CW test facility in operation in the vicinity of ITER site to test and qualify ICRH antenna components in ITER relevant condition. TITAN is designed to host up to a quarter of an ITER antenna (10 tons) and to test antenna or diagnostics components (rear vacuum transmission line, sliding contacts, four port junction, RF window…). It consists of a vacuum vessel, a cooling/baking water loop, high power 35–80MHz RF sources and a RF matching system. The vacuum vessel is used to test large components and subsystems in high vacuum conditions at relevant temperature corresponding to ITER operating conditions. The volume is close to 17.5 m^3 (≈ 4m length x 2.7 m diameter)

for a total weight of 7 T. It can reach 10^{-5} Pa in 48hours. The RF matching system is based on a cooled T resonator. The main technical issue of this system is the CW operation. The matching system is a mandatory sub-system of the RF test facility to qualify most of the critical components for ITER antenna such as.
The first and successful exploitation of TITAN has been performed in February 2011 to qualify a Tore Supra antenna (combined vacuum leak and RF tests) prior to its installation on the machine (Fig. 4 (right)). The Tore Supra antenna with new generation of Faraday screen (c.f. section 2) has been installed on the TITAN vacuum vessel. Contrary to past operation, TITAN offers a unique combination of vacuum leak and RF tests on the same test bed. Thanks to the very good pumping efficiency of the vacuum vessel, a fast recovery of pressure after RF pulses has been recorded. This property enables us to save experimental time on the test bed by reducing the time interval between two RF tests. In the example shown on Fig. 4 (right), RF pulses have been obtained at 40kV up to 5s with different antenna temperature: either at the ambient temperature (20°C) or at ~100°C. Since then, TITAN has been successfully qualified for routine and long pulse operation: up to ~1000s RF pulse with the Tore Supra ICRH antenna operating at 20kV/57MHz.

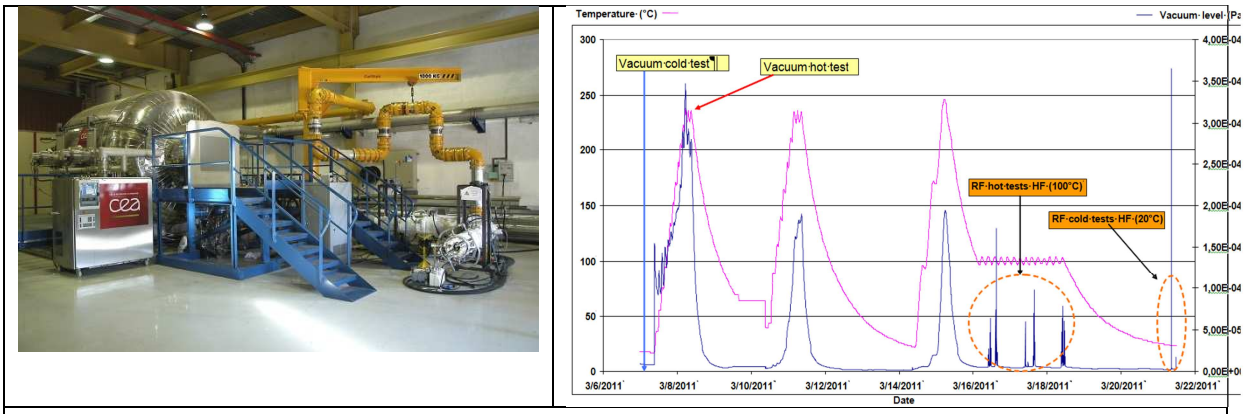

Fig. 4*:(left) picture of TITAN facility. (right) TITAN operation: record of vessel temperature (pink line °C) and vessel pressure (blue line Pa) versus calendar date.*

5. A new approach to ITER–ICRH loads for antenna laboratory testing

One way of improving the commissioning of ICRH antennae on test facility is the upgrading of the load testing performances. Indeed, low permittivity ($\varepsilon' \leq 81$) salted water loads commonly used on low power test-bed exhibit some limitations. High permittivity materials like ferroelectric barium titanate, $BaTiO_3$, ceramic powders are identified as promising way to mimic suitable plasma-like conditions at low costs and reduced complexity [23]. This approach is aiming at a significant improvement of the ICRF laboratory tests in view of saving experimental time on tokamaks usually dedicated to antenna commissioning. The dielectric constant $\varepsilon = \varepsilon' + i\varepsilon''$ of sintered BaT_iO_3 ceramic powder and BaT_iO_3 ceramic powder mixed with either water or salted water has been experimentally characterized within a large frequency domain covering the operation range of both ITER ICRF antenna at 40-55 MHz and the ITER scaled-down mock-up at 160-220LPP-ERM/KMS Such materials offer a large range of permittivity from 230 to 1880 at 50 MHz.
A load with dielectric constant ~200 above cut-off frequency is expected to provide a plasma-like response over all the frequency range and for all antenna phasings [24-25]. With a permittivity lying between 200 and 400 at 200 MHz for the scaled-down antenna mock-up, BaT_iO_3 ceramic powder mixed with either water or salted water meet the requirements for upgrading loads currently used. The antenna behavior with such loads has been numerically

checked. The simulation indicates a good description of the frequency response to ITER reference plasma profile even for the toroidal phasing [0 π 0 π] as the low frequency part of the radiated spectrum is no more evanescent. The coupling resistance is adjusted by either the antenna-load distance or the salt concentration.
In a near future, it is planned to characterize the ITER antenna mock-up at LPP-ERM/KMS with an ICRH load consisting of BaT_iO_3 ceramic powder mixed with salted water. The proposed solution offers the best trade-off between coupling capabilities and the good wave absorption. The size of the load tank to be installed in front of the antenna is designed to avoid standing wave patterns, following RF simulation of the antenna-load coupling behavior. ITER ICRH antenna response will be extrapolated from the scaled-down mock-up experiments as long as the dielectric constant of the ITER load at 50MHz is the same as the one of the mock-up load at 200MHz [26]. Finally, by adjusting the salt concentration in the BaT_iO_3 mixture it is possible to design ICRF loads with suitable dielectric constant within the 40-55MHz range to test the full size ITER antenna.

Acknowledgment: Part of this work, supported by the European Communities under the contract of Association between EURATOM and CEA, was carried out within the framework of the European Fusion Development Agreement. The views and opinions expressed herein do not necessarily reflect those of the European Commission. The new test stand facility, TITAN, was supported within the framework of the French government stimulus plan 2010.

References:

[1] Perkins F.W., *Nucl. Fusion* **29** (1989) 583
[2] Mendes A, L. Colas L et al *Nucl. Fusion* **50** (2010) 025021
[3] Corre Y. et al. accepted to *Nuclear Fusion* (2012)
[4] Kubič M. et al., proc. ICONE conf. Anaheim 2012
[5] Ritz G.et al. Proc. 27th SOFT conf. Liège 2012, submitted to *FED*
[6] Colas L. et al Proc. 20th PSI conf. Aachen 2012 P1-5, submitted to *JNM*
[7] Jacquot J., Milanesio D. et al., proc. 39th EPS conf. on Plasma Physics & Cont. Fusion, Stockholm 2012, P2.038, http://ocs.ciemat.es/EPSICPP2012PAP/pdf/P2.038.pdf
[8] Colas L., Jacquot J. et al. accepted in *Physics of Plasmas* (2012)
[9] D'Ippolito D.A. & Myra J.R., *Physics of Plasmas* **13** (2006)102508
[10] Lancellotti V., Milanesio D. et al., *Nucl. Fusion* **46** (2006) S476–S499
[11] Bernard J.M. et al. proc. 27th SOFT conf. Liège 2012, submitted to *FED*
[12] Lerche E. et al., proc. 18th RF top. Conf. Ghent 2009, AIP CP **1187** 93
[13] Dumont R.J. and Zarzoso D., submitted to Nucl. Fusion 2012
[14] Petty C.C. et al , Nucl. Fusion **39** (1999) 1421
[15] Hellsten T. et al, Nucl. Fusion **45** (2005) 706
[16] Bécoulet A., Plasma Phys. Control. Fusion **38** (1996) A1
[17] Bergeaud V., Eriksson L.-G. and Start D. F. H., Nucl. Fusion **40** (2000) 35
[18] Dumont R.J., Nucl. Fusion **49** (2009) 075033
[19] Ehst D.A. and Karney C.F.F., Nucl. Fusion **31** (1991) 1933
[20] Bilato R., Brambilla M., Pavlenko I. and Meo F., Nucl. Fusion **42** (2002) 1085
[21] Budny R.V. et al Nucl. Fusion **52** (2012) 023023
[22] Bernard J.M. et al Fus Eng. & Des. **86** (2011) 876
[23] Bottollier-Curtet H. et al. Fusion Eng. & Des. **86** (2011) 2651
[24] Messiaen A. et al. Fusion Eng. & Des. **86** (2011) 855
[25] Champeaux S. et al. 19th Top. Conf. on Radio-Frequency Power in Plasmas, AIP Conference Proceedings, vol. 1406, Newport, USA (2011) 41
[26] Messiaen A. et al. Fusion Eng. & Des. **74** (2005) 367